Journal of Constructional Steel Research 87 (2013) 38–47

Contents lists available at SciVerse ScienceDirect

Journal of Constructional Steel Research

Internal flange stiffened moment connections with low-damage capability under seismic loading

Chung-Che Chou [a,b,*], Sheng-Wei Lo [c], Gin-Show Liou [c]

[a] Department of Civil Engineering, National Taiwan University, Taipei, Taiwan
[b] National Center for Research on Earthquake Engineering, Taipei, Taiwan
[c] Department of Civil Engineering, National Chiao Tung University, Hsinchu, Taiwan

ARTICLE INFO

Article history:
Received 30 October 2012
Accepted 14 April 2013
Available online 17 May 2013

Keywords:
IFS steel moment connection
Low-damage capability
Test
Finite element analysis

ABSTRACT

This study presents the seismic performance of steel moment connections using internal flange stiffeners (IFSs) welded at the face of the wide-flange column and inner side of the beam flange. The objective is to develop a steel moment connection that can achieve good seismic performance with low-damage capability during a large earthquake loading and minimize the repair cost. Four large-scale moment connections were tested to validate the cyclic performance. One connection which represented a welded-unreinforced flange-bolted web connection failed before finishing cyclic tests at a drift of 4%. Three IFS moment connections showed excellent performance and low damage after experiencing the AISC seismic load twice up to the target drift of 4%, without strength reduction. The specimens were also modeled using the computer program ABAQUS to further verify the effectiveness of the IFS in transferring beam moment to the column and to investigate potential sources of connection failure.

1. Introduction

The widespread damage of welded steel moment connections after the 1994 Northridge earthquake and 1995 Hyogoken-Nanbu (Kobe) earthquake initiates extensive research aimed at improving connection seismic performance. Many traditional steel moment connections, which were fabricated following pre-Northridge construction practices with a low notch toughness E70T-4 electrode, show minimal plastic deformation (e.g., 1% drift) before weld fracture at the beam-to-column interface [1–4]. By using a high notch toughness electrode for connection welds, strengthening or reducing the beam end section [5–10] are also needed for most qualified moment connections to reach a required seismic performance. FEMA 350 [11] lists some prequalified moment connections for the special moment frame (SMF). These moment connections are capable of sustaining an interstory drift of at least 4% with sufficient flexural resistance [12]. However, high damage in the beam (e.g., buckling) after seismic loading leads to a large cost for repair.

Adding a pair of full-depth side plates or separate internal flange stiffeners (IFSs) between the column face and beam flange inner side has been demonstrated as an alternative to achieve good seismic performance of moment connections [13,14]. This scheme not only minimizes the interference from the composite slab but also reduces story height requirements in the building. Test results showed that the IFS moment connection experiences very minor beam local buckling (e.g., low damage) during the code-specified cyclic loading [12] in excess of a 4% drift. The connection requires minor repair and has the capability to sustain the same cyclic loading again to a drift of 4% without failure, showing repeatable seismic performance as observed in the first test. However, previous studies focused only on the IFS moment connection with a steel built-up box column and a wide flange beam, which are commonly used in Asian countries to resist seismic loads in SMFs. The use of a wide-flange column is also very popular in SMFs, but the load-transfer from IFSs to the box column is more effective than that to the wide-flange column due to two web plates in the box column. Moreover, previous specimens used the ASTM A36 steel beam, which produces smaller stresses in connection welds than the ASTM A572 Gr. 50 steel beam. Therefore, the specific connection configuration in this study uses a wide-flange column and a beam with various material properties. To design a moment connection with low-damage capability under seismic loading, four IFSs, each of which is a rectangular or triangular flat plate, are welded at the column face and beam flange inner side to help transfer some beam flange force to the column. The objective of the study is to examine alternative technique for the moment connection with a wide-flange column and beam to improve the fracture resistance through strengthening of connections.

A total of four large-scale exterior moment connections were tested. Test parameters were IFS sizes and material properties of the beam. One welded-unreinforced flange-bolted web connection was tested as a benchmark. Three moment connections with different IFSs and beam materials were tested to validate their cyclic performances. The study showed that all IFS moment connection specimens performed much better than a non-stiffened moment connection specimen, even being tested twice up to a 5% drift. These specimens were also modeled

* Corresponding author. Tel.: +886 2 3366 4349; fax: +886 2 2739 6752.
E-mail address: cechou@ntu.edu.tw (C.-C. Chou).

0143-974X/$ – see front matter © 2013 Elsevier Ltd. All rights reserved.
http://dx.doi.org/10.1016/j.jcsr.2013.04.005

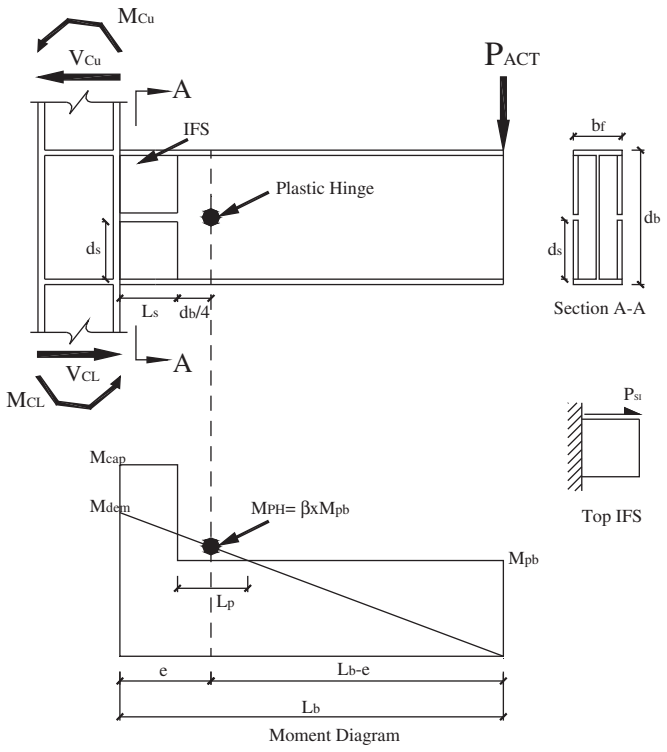

Fig. 1. Moment capacity and demand of the beam.

using the computer program ABAQUS [15] to further verify the effectiveness of the IFS in transferring beam moment to the column and to investigate potential sources of connection failure. This paper presents experimentally and analytically the cyclic behavior of the IFS moment connection, and provides recommendations for seismic design of such connections.

2. IFS moment connection

2.1. Connection design

Fig. 1 shows a moment connection with IFSs. The purpose in using IFSs is to transfer some not all beam flange force to the column because existing beam flange groove welded joints conducted by the high toughness electrode can sustain modest inelastic deformation before fractures. Moment demand, M_{dem}, along the beam is shown in the figure, assuming that a plastic hinge is located at a quarter beam depth from the IFS end. This location is used based on previous connection test results [13,14]. The moment at the column face, determined by projecting moment capacity M_{PH} at the plastic hinge section, is

$$M_{dem} = \frac{L_b}{L_b-(L_s+d_b/4)}M_{PH} = \frac{L_b}{L_b-(L_s+d_b/4)}\left(\beta R_y \sigma_{yn} Z_b\right) \quad (1)$$

where L_b is the distance from the actuator to the column face; L_s is the IFS length, which assumes half the beam depth in initial design; d_b is the beam depth; Z_b is the plastic section modulus of the beam; σ_{yn} is the specified yield strength of the steel; R_y is the material overstrength coefficient, and coefficient β accounts for strain hardening [11].

Moment capacity near the beam-to-column interface increases due to presence of IFSs. The flexural capacity of the stiffened beam, M_{cap}, is the summation of flexural strengths of the beam, M_{pb}, and the IFSs, M_{ps} [13]:

$$M_{cap} = M_{pb} + M_{ps} = Z_b R_y \sigma_{yn} + 2\left(2\sqrt{\frac{1}{2}}-1\right)\left(d_b-2t_f\right)R_y\sigma_{yn}d_s t_s \quad (2)$$

where t_f is the beam flange thickness; d_s is the IFS depth, and t_s is the IFS thickness. Assuming that the stiffened beam moment capacity–demand ratio, α ($=M_{cap}/M_{dem}$), is larger than 1.05, the IFS size can be determined by:

$$d_s t_s \geq \frac{\alpha M_{dem} - M_{pb}}{2\left(2\sqrt{\frac{1}{2}}-1\right)\left(d_b-2t_f\right)R_y\sigma_{yn}}. \quad (3)$$

Since the force in the IFS, P_{SI}, is transferred through shear on the groove welded joint between the IFS and beam flange inner side, the length of the IFS, L_s, is determined based on shear strength of the IFS:

$$L_s \geq \frac{P_{SI}}{0.9\left(0.6R_y\sigma_{yn}\right)t_s} = \frac{\left(2\sqrt{\frac{1}{2}}-1\right)R_y\sigma_{yn}t_s d_s}{0.9\left(0.6R_y\sigma_{yn}\right)t_s} = 0.77d_s. \quad (4)$$

Table 1
Member sizes and properties.

(a) Specimen sizes

Specimen	Column size	Beam size	IFS size ($t_s \times d_s \times L_s$)	$\frac{\sum M^*_{pc}}{\sum M^*_{pb}}$
UR	H428 × 407 × 20 × 35	H702 × 254 × 16 × 28	–	1.72
IFS1	(A572 Gr. 50)	(A36)	R25 × 308 × 300	1.53
IFS2			T20 × 308 × 300	1.47
IFS3		H702 × 254 × 16 × 28 (A572 Gr.50)	T28 × 308 × 300	1.19

$\sum M^*_{pc}$ = sum of the column nominal moments at the top and bottom of the panel zone.
$\sum M^*_{pb}$ = sum of the beam moments resulting from the beam plastic hinge moment.

(b) Material properties

Specimen	Column strength (MPa)				Beam strength (MPa)				IFS strength (MPa)	
	Flange		Web		Flange		Web			
	σ_y	σ_u	σ_y	σ_u	σ_y	σ_u	σ_y	σ_u	σ_y	σ_u
UR	357	521	390	510	251	463	285	453	–	
IFS1									409	528
IFS2					272	469	275	440	421	527
IFS3					388	531	417	564	388	531

σ_y = Yield strength; σ_u = Ultimate strength.

The IFS size can be determined based on Eqs. (3) and (4). Iterate over a new L_s by returning to Eq. (1) if Eq. (4) is not satisfied.

3. Test program

3.1. Specimens

The experimental program consisted of tests of four specimens. Each specimen represented an exterior moment connection with one steel beam (H702 × 254 × 16 × 28) and one wide-flange column (H428 × 407 × 20 × 35). Table 1 shows specimen sizes and material properties obtained from coupon tensile tests. ASTM A572 Gr. 50 steel was utilized for all columns and internal flange stiffeners. ASTM A36 steel was utilized for the beams of Specimens UR, IFS1, and IFS2; ASTM A572 Gr. 50 steel was utilized for the beam of Specimen IFS 3. These two types of steel were manufactured in Taiwan, conforming to chemical and mechanical properties of ASTM standards [16]. All connections were welded using the ER70S-G electrode, which is similar to the high-toughness E71T-8 or E70TG-K2 electrodes and provides a minimum specified Charpy V-Notch value of 27 J at −29 °C (20 ft-lb at −20 °F). The steel backing bars projected 30 mm beyond both sides of the beam flange and no weld tabs were used. The steel backing bar was left in place and a fillet weld, helping to reduce the notch effect of a left in place backing bar [11], was not made between the backing bar and column. Each pass of flange groove welds was initiated and terminated at a point outside the flange. This was done to prevent poor-quality welds, which normally occur at the initiation of the weld. All specimens were made by a fabrication shop welder, using weld positions typical to field welding. More specifically, beam flange groove welds were made with the specimen oriented to permit flat position welding. Ultrasonic tests (UT) were conducted for all flange groove welds, and they all satisfied the prescribed acceptance criteria [17]. Only A490 high-strength bolts were used to connect the column shear tab and beam web.

Specimen UR used a welded-unreinforced flange-bolted web connection (Fig. 2(a)). Specimen IFS1 was identical to Specimen UR, except that the 25-mm thick rectangular IFSs were used at the beam flange edges of Specimen IFS1 [Fig. 2(b)]. Specimen IFS2 was identical to Specimen IFS1, except that the 20-mm thick triangular IFSs were

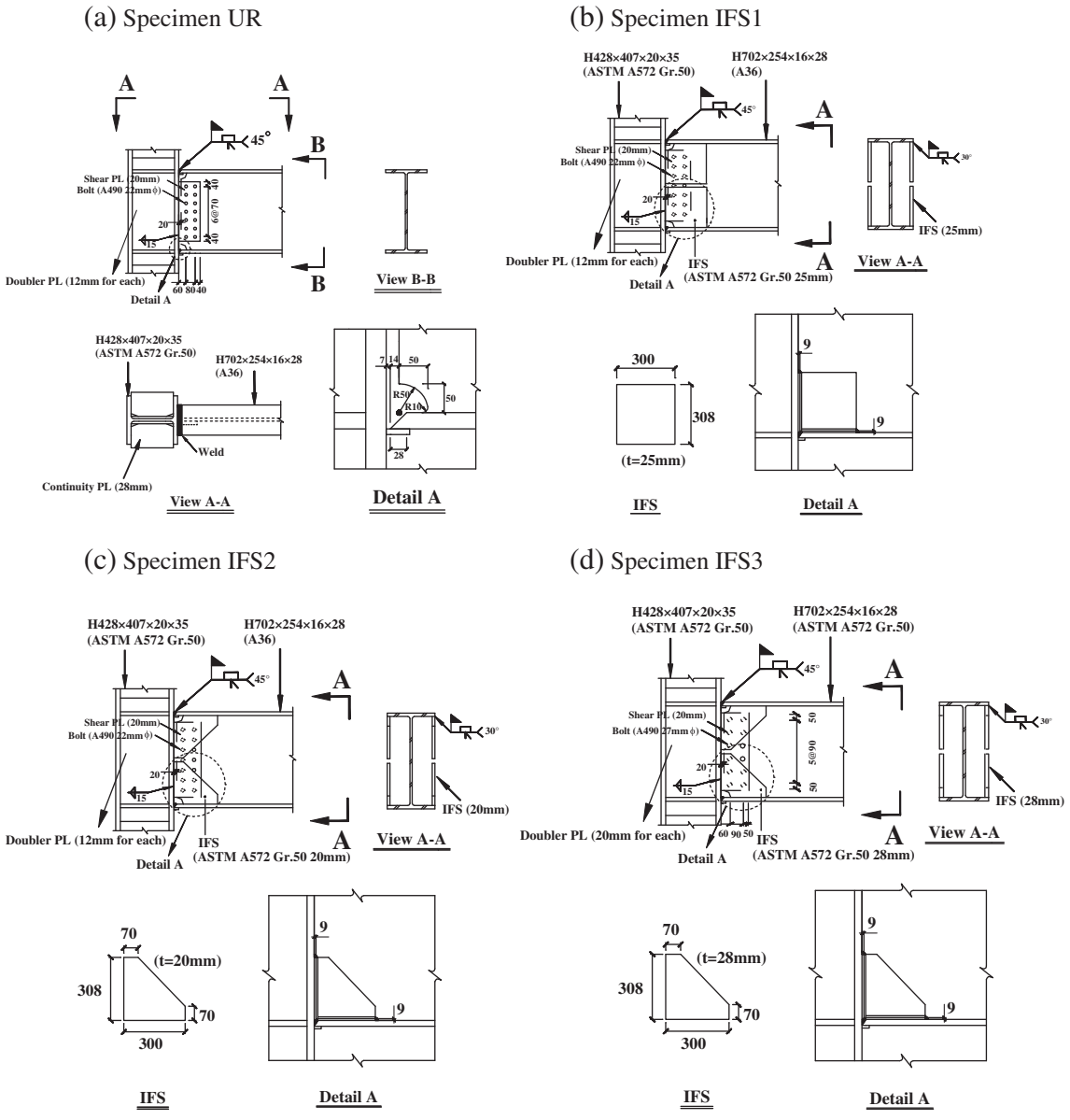

Fig. 2. Connection details.

Table 2
Beam moment capacity–demand ratio.

Specimen	M_{pb}	M_{ps}	M_{cap}	M_{dem}	M_{PH}	α	β
	(kN-m)						
IFS1	1679	1685	3364	2810	2457	1.20	1.46
IFS2	1763	1388	3151	2983	2608	1.06	1.48
IFS3	2556	1791	4347	3663	3203	1.19	1.25

Note: Moment is calculated based on the actuator force at an interstory drift of 4%.

used at the beam flange edges of Specimen IFS2 [Fig. 2(c)]. Thinner IFSs in Specimen IFS2 leaded to less welding and smaller beam moment capacity–demand ratio, α, as listed in Table 2. Specimen IFS3 [Fig. 2(d)] was identical to Specimen IFS2, except that Specimen IFS3 had the ASTM A572 Gr. 50 steel beam and thick triangular IFSs (Table 1(a)). The beam moment capacity–demand ratio, α ($=M_{cap}/M_{dem}$), ranged from 1.06 to 1.20 (Table 2) to study the effects of IFSs on the connection behavior. Doubler plates were added in the column to maintain a strong panel zone; in other words, the panel zone shear computed based on the beam plastic hinge moment, M_{PH}, was less than 60% panel zone shear strength, V_p, [12]:

$$V_p = \left(0.6\sigma_{yn} d_c t_{total}\right)\left[1 + \frac{3b_{cf}t_{cf}^2}{d_h d_c t_{total}}\right] \quad (5)$$

where t_{cf} is the column flange thickness; b_{cf} is the column flange width; d_h is the panel zone depth; d_c is the column depth, and t_{total} is the total thickness of the column web and doubler plates.

3.2. Test setup and loading protocol

The exterior connection specimens were tested as shown in Fig. 3. Restraint to lateral-torsional buckling of the beam was provided near the actuator and at a distance of 2000 mm from the column centerline. Displacements were imposed on the beam by actuators at a distance of 4000 mm from the column centerline. The AISC cyclic displacement history [12] was used and run under displacement control. The intersory drift, which was computed by the actuator displacement divided by the distance to the column centerline, was used as the control variable. Specimens were tested until connection failure occurred.

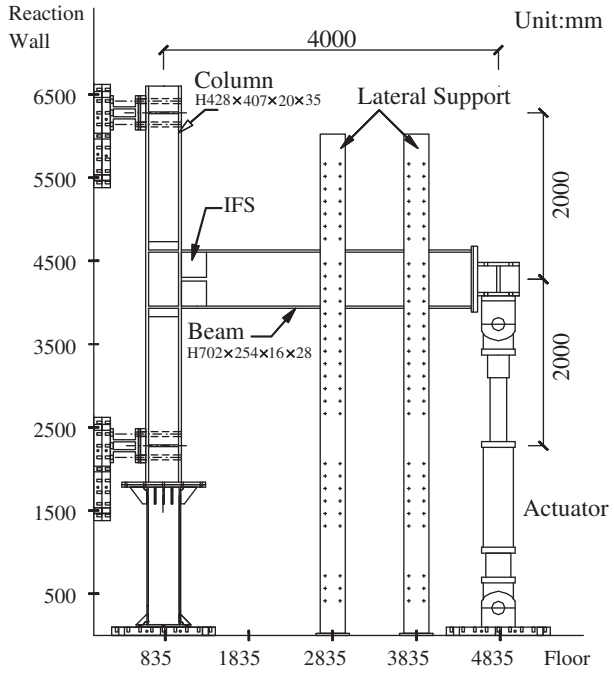

Fig. 3. Test setup (unit: mm).

4. Test results

4.1. Welded-unreinforced flange-bolted web connection

Fig. 4(a) shows the global response of Specimen UR; the moment computed at the column face is normalized by the nominal plastic moment of the beam, M_{np} ($=Z_b\sigma_{yn}$). Whitewash flaking was observed in the beam flange at an interstory drift of 0.75%, indicating beam yield. A minor fracture occurred in the beam top flange groove weld at an interstory drift of −2%, but the peak strength was maintained at this drift level. A significant reduction in strength occurred toward the second cycle of an interstory drift of −4% due to beam top flange fracture (Fig. 5). No yielding of the column or panel zone was observed throughout the test. Although Specimen UR utilized the ASTM A36 beam, the connection failed before finishing cyclic tests at a drift of 4%.

4.2. Internal flange stiffened moment connection

All IFS connections performed well under the first cyclic test, exhibiting no groove-weld failures at an interstory drift of 4%. The low damage (e.g., minor buckling) in the beam did not need repair after the first test, so all IFS specimens were tested again using the same loading protocol, exhibiting similar cyclic performances as observed in the first test up to an interstory drift of 4% [Fig. 4(b)–(d)].

Specimens IFS1 and IFS2 were identical to Specimen UR, except that (1) the 25-mm thick rectangular IFSs were used for Specimen IFS1, and (2) the 20-mm thick triangular IFSs were used for Specimen IFS2. Specimens IFS1 and IFS2, which had beam capacity–demand ratios of 1.2 and 1.06, respectively, were used to evaluate the effects of IFS sizes on the connection behavior. Two specimens showed similar cyclic behaviors during the first test. Yielding, observed by whitewash flaking, occurred at an interstory drift of 0.75%, concentrated outside the IFS. After finishing 4% drift cycles, yielding extended more than 1000 mm from the column face with sign of minor flange buckling (Figs. 6(a) and 7(a)). A minor fracture occurred at the end of welds between the IFS and beam top flange. The weld crack was repaired before conducting the second test. For subsequent loading cycles, Specimen IFS1 achieved a maximum interstory drift of 5% with beam local buckling (Fig. 6(b)) and no groove weld fracture. For Specimen IFS2 in the second test, a minor crack occurred in the beam top flange near groove welds at a drift of −1%, but it did not affect the connection performance after finishing the first cycle of 5% drift [Fig. 7(b)]. The beam top flange fractured when the connection moved toward the second cycle of −5% drift. This indicates that the connection with thicker IFSs can provide better cyclic performance in the second cyclic test.

Specimen IFS3 used the ASTM A572 Gr. 50 steel beam, so its IFS size was thicker than other specimens with the ASTM A36 beams to maintain similar beam capacity–demand ratios (Table 2). Since beam local buckling was minor and no strength degradation was observed after the first cyclic test (Fig. 8(a)), Specimen IFS3 was also retested using the same AISC loading protocol [12]. Beam local buckling became obvious at an interstory drift of 3%, but the peak strength was maintained after finishing two cycles of 5% drift without failure (Fig. 4(d)). Beam buckling accompanied by twisting resulted in a small reduction in beam flexural strength at a first cycle of 6% drift [Figs. 8(b) and 4(d)]. Meanwhile, a minor fracture in the groove weld was observed near the beam bottom flange to the column face. A significant reduction in strength occurred toward a second cycle of 6% drift due to beam bottom flange fracture (Fig. 8(c) and 4(d)). No yielding of the column or panel zone was observed throughout the test. The performance of Specimen IFS3 in the second cyclic test also

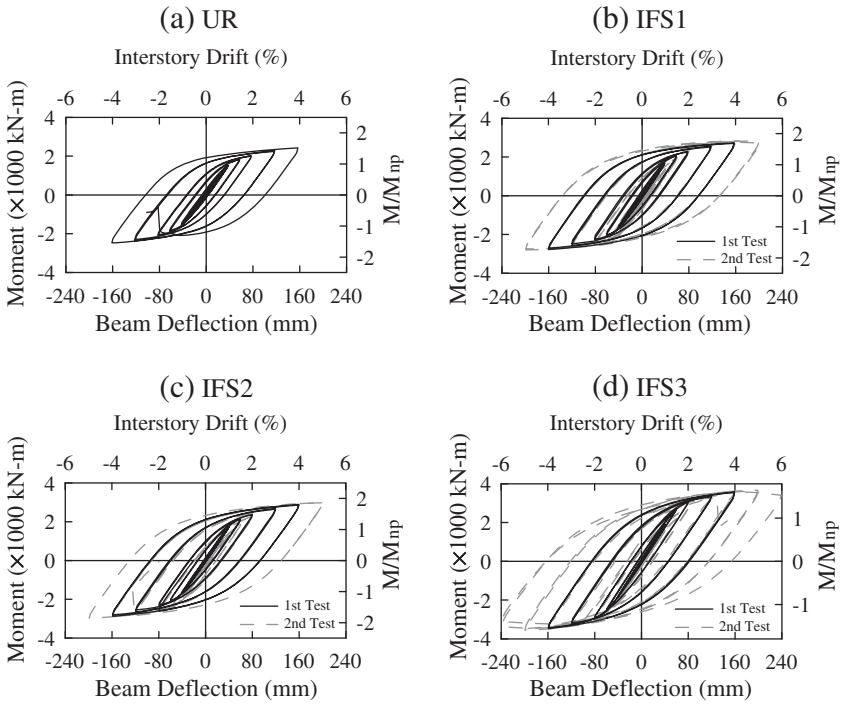

Fig. 4. Beam moment-deflection responses.

exceeds stringent requirements based on AISC seismic provisions [12]. The test results indicate that as long as the IFS is designed properly, it can reduce stress concentration in groove welds and delay weld fractures to a drift level much higher than 4%. Specimens IFS1 and IFS3 with a similar beam capacity demand ratio, $\alpha = 1.2$ (Table 2), showed comparable deformation capacities irrespective of shapes of the IFS and beam material properties. The maximum moment developed at the assumed plastic hinge location was 1.25–1.48 times the beam's actual plastic moment (Table 2); the value of strain hardening, β, was larger for the ASTM A36 beam (Specimens IFS1 and IFS2) than for the ASTM A572 Gr. 50 beam (Specimen IFS3). The strain hardening of around 1.5 for the ASTM A36 beam exceeded that calculated based on FEMA 350 [11] due to minor beam local buckling at the plastic hinge location in the test.

4.3. Beam flange strains

The effectiveness of the IFS in decreasing beam flange tensile strain can be observed from the measured strain at a distance of 60 mm from the column face (Fig. 9(a)). At an interstory drift of 4%, the tensile strains in the beam top flange of Specimen UR range from 6 to 12%, much higher than those of the IFS moment connections. The maximum tensile strain of Specimens IFS1-3 at an interstory drift of 4% was about

Fig. 5. Specimen UR beam top flange fracture (first test).

(a) First Test to +4% Drift (Second Cycle)

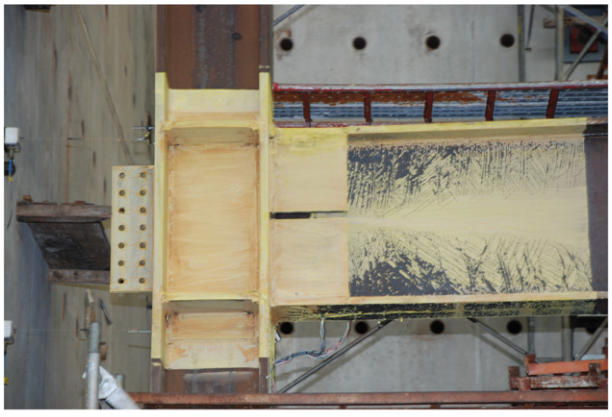

(b) Second Test to -5% Drift (Second Cycle)

Fig. 6. Specimen IFS1 observed performance.

(a) First Test to +4% Drift (Second Cycle)

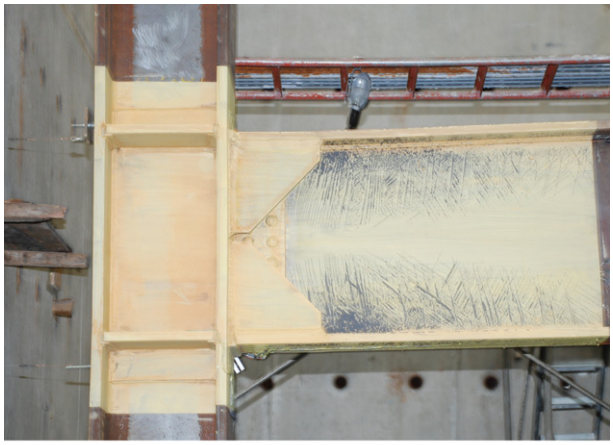

(b) Second Test to +5% Drift (First Cycle)

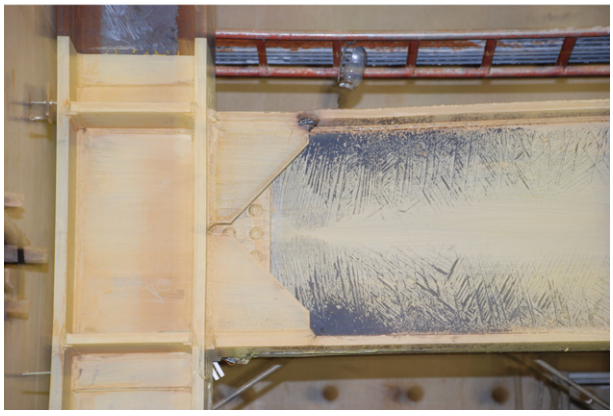

Fig. 7. Specimen IFS2 observed performance.

(a) Strain Profiles across Beam Width

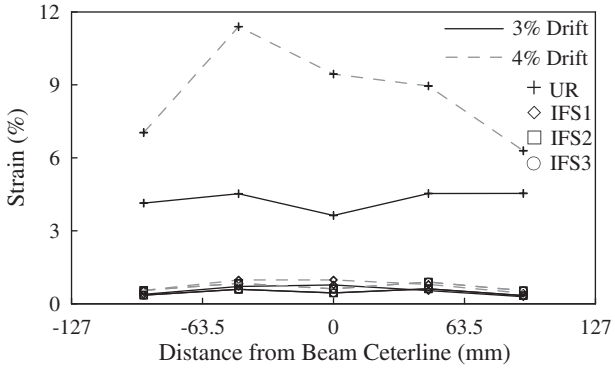

(b) Strain Profiles along a Beam Axis

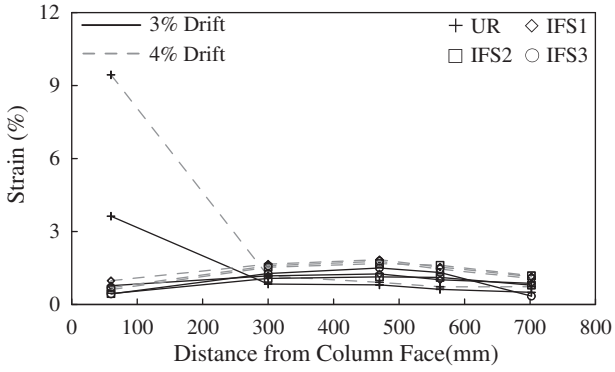

Fig. 9. Beam bottom flange strain profiles.

(a) First Test to +4% Drift (Second Cycle)

(c) Second Test to +6% Drift (Second Cycle)

(b) Second Test to -6% Drift (First Cycle)

Fig. 8. Specimen IFS3 observed performance.

1%, indicating that the IFS was effective in reducing strain demand and thereby delayed brittle fracture of the connection to a drift higher than 4%.

Fig. 9(b) shows flange strains along the beam axis of all specimens. Maximum tensile strains of Specimens UR and IFS1-3 occurred near the column face and beyond the end of the IFS, respectively. At an interstory drift of 4%, maximum strain at the assumed location of the beam plastic hinge in IFS connections, which was about 476 mm ($=L_s + d_b/4$) away from the column face, was about $9\varepsilon_y$ in tension and $6\varepsilon_y$ in compression, demonstrating successful relocation of the plastic hinge away from the column face.

4.4. Internal flange stiffener strains

Fig. 10 presents the measured longitudinal strains along the stiffener depth, 35 mm from the column face. Experimental observations were that (1) longitudinal strains beyond the neutral axis of the IFS have values opposite those of the IFS side connecting the beam flange, and (2) longitudinal strains near the beam flange are greater than yield strain at a drift of 4%. Because Specimen IFS2 had weaker stiffeners than Specimen IFS1, the tensile strain in the IFS near the beam flange was higher in Specimen IFS2 than in Specimen IFS1. For Specimen IFS3 with the ASTM A572 Gr. 50 beam, much higher tensile strain could be observed as compared to Specimens IFS1 and IFS2 with the ASTM A36 beam. The maximum measured tensile strain at an interstory drift of 4% was $1.5\varepsilon_y$ in Specimen IFS3.

5. Analytical study

The finite element models were prepared for Specimens UR, IFS1, IFS2, and IFS3 using the finite element analysis program ABAQUS [15] to study the effectiveness of the IFS in transferring beam moment to the column and sources of potential failure mode. Fig. 11(a) shows the finite element model consisting of eight-node brick elements C3D8R that use standard integration. The groove welds joining the beam flange and column were also modeled (Fig. 11(b)). The geometry of beam flange groove welds in the model was considered based on the flange bevel angle and gap between the beam flange and the column. The steel backing was not modeled. Coordinates common to components joined by the shear tab and beam web were constrained such that they had identical displacements. Material properties used for the models were taken from coupon tensile tests (Table 1(b)). The stress–strain curve was approximated by a bi-linear relationship. No residual stresses of groove welds were taken into account in the modeling. The analyses accounted for material nonlinearities, using the von Mises yield criterion. Combined isotropic and kinematic hardening was assumed for the cyclic analysis; the parameters for modeling were obtained based on previous research [18].

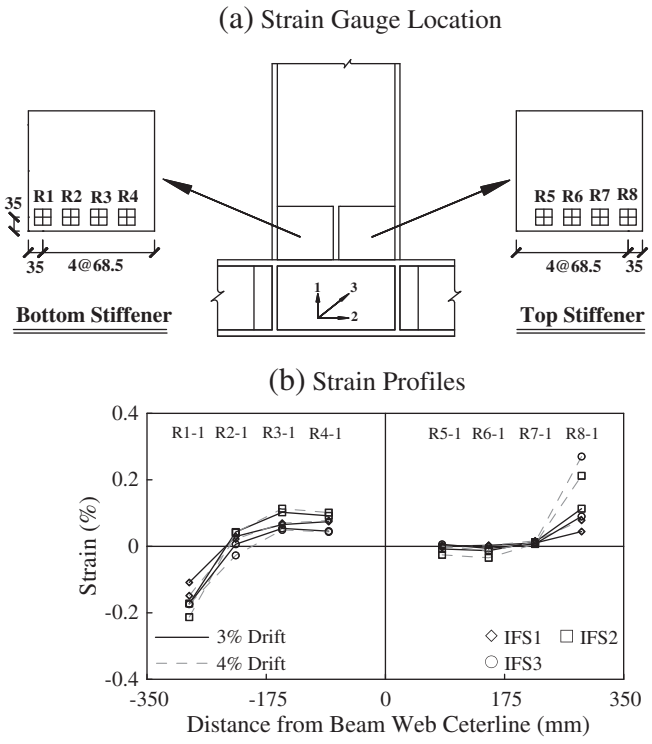

Fig. 10. IFS strain profiles (35 mm away from the column face).

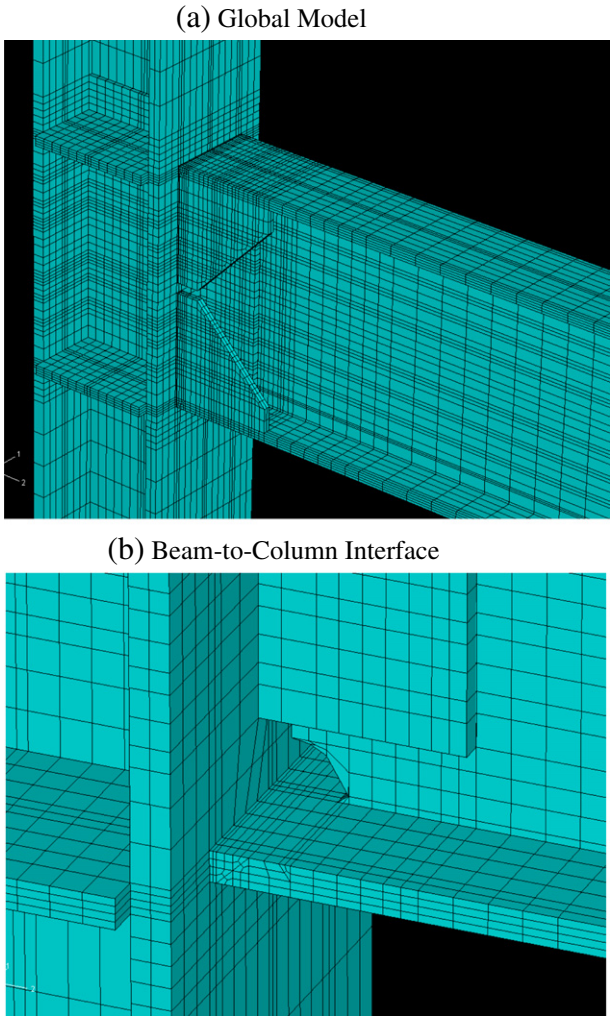

Fig. 11. Finite element model.

Fig. 12 shows comparisons of beam moment-deflection hysteretic responses from the test and analysis. Both initial stiffness and post-yield results show reasonable agreement with test data. Fig. 13 shows longitudinal strains in the IFS from the test and analysis, indicating that the force transfer from the IFS to the column can be correlated well from the finite element model. Moment, M_s, transferred through the IFS to the column was computed from longitudinal stresses along the IFS depth, the respective sectional area, and distance to beam web centerline. The ratio of M_s to connection moment, M_{ABA}, computed at the column face, increased with drift (Fig. 14). Specimen IFS1 showed higher moment resistance of the IFS than Specimen IFS2 because a stiffener with increased thickness helps transfer a larger moment from the beam flange to the column. At an

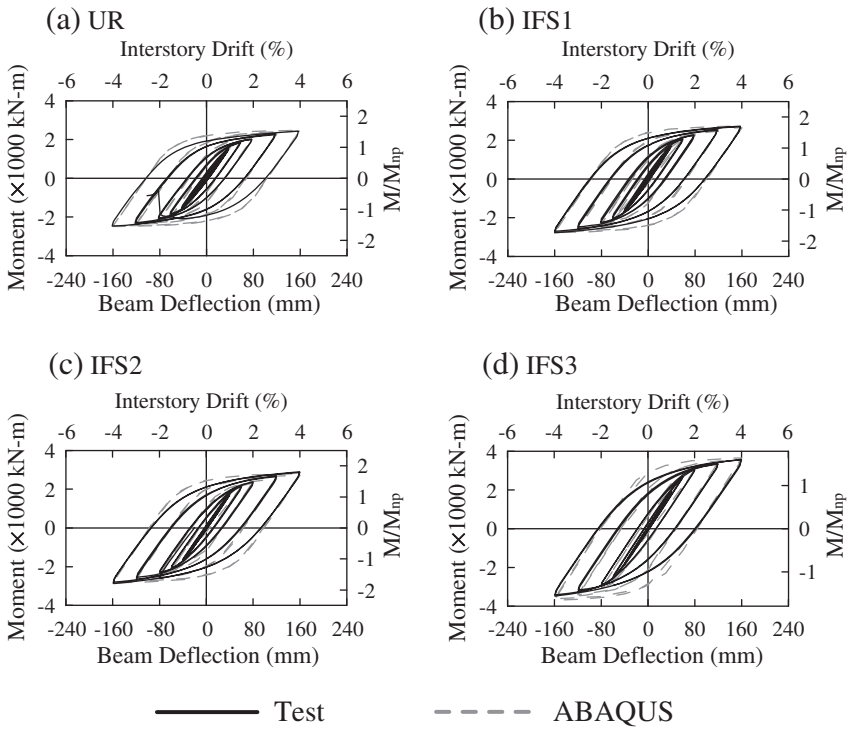

Fig. 12. Comparison of hysteresis responses from the first test and ABAQUS analysis.

interstory drift of 4%, this moment ratio was about 20–25%, lower than that obtained from the IFS moment connections with a steel built-up box column and beam. It suggests that the web plate located at both sides of the box column is more effective than that located in the center of the wide-flange column to transfer the IFS moment from the beam to the column.

The rupture index (RI) is computed at different locations of the connection from ABAQUS results to assess the possible source of fracture. The RI equals the product of a material constant and the PEEQ (plastic equivalent strain) divided by the strain at the ductile fracture, ε_r, which is given by Hancock and Mackenzie [19]:

$$\mathrm{RI} = \frac{a\mathrm{PEEQ}}{\varepsilon_r} = \frac{\sqrt{\frac{2}{3}\varepsilon_{ij}^{p}\varepsilon_{ij}^{p}}/\varepsilon_y}{\exp\left(-1.5\frac{\sigma_m}{\sigma_{eff}}\right)} \tag{6}$$

where ε_{ij}^{p} is the plastic strain components; σ_m is the hydrostatic stress, and σ_{eff} is the von Mises stress. Therefore, locations in a connection with high RI values have a high potential for fracture. Fig. 15(a) shows three possible fracture locations observed in the tests: the beam flange top surface located 60 mm from the column face (Line A), the groove-weld top surface near the column face (Line B), and the beam flange inner side along the weld between the IFS and beam flange (Line C). The RI values can be significantly reduced at the beam flange near the column face by providing the IFS [Fig. 15(b)]. The maximum RI value for Specimens IFS1-3 at both ends of the beam flange groove weld is higher than that for Specimen UR [Fig. 15(c)] because the IFSs are positioned at both edges of the beam flange to transfer beam flange force to the column. Moreover, Specimen IFS3 with the ASTM A572 Gr. 50 beam has flexural capacity much higher than other specimens with the ASTM A36 beam, so it has the highest RI value among all specimens. Although the RI value at the IFS location increases, it is still lower than the fracture limit due to no weld fractures before an interstory drift of 5% in the test. The RI value at the end of the IFS-to-beam flange also increases [Fig. 15(d)], indicating another possible source of fracture as observed in the first test of Specimens IFS1 and IFS2.

6. Conclusions

Four large-scale exterior moment connection specimens, each composed of the ASTM A572 Gr. 50 H428 × 407 × 20 × 35 column and the H702 × 254 × 16 × 28 beam, were tested and analyzed to verify their seismic performance. The objective was to evaluate the

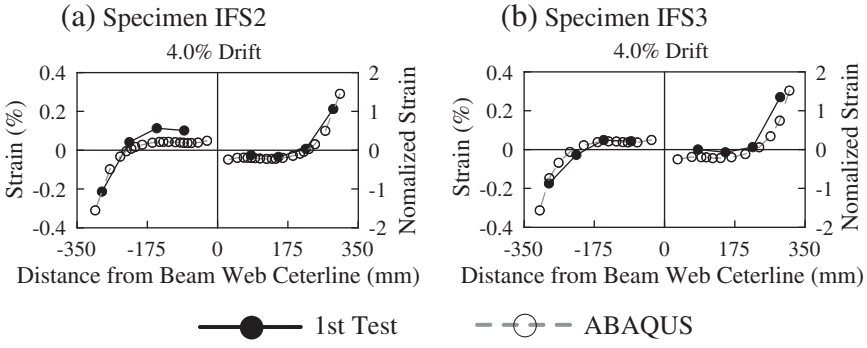

Fig. 13. Comparison of IFS strain profiles from test and ABAQUS analysis.

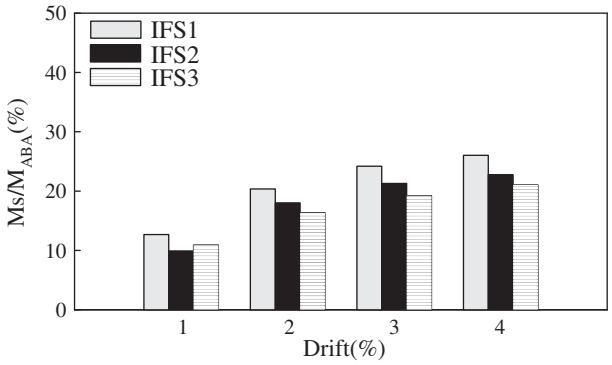

Fig. 14. IFS moment contribution ratio (positive bending).

IFS moment connection with low-damage capability under the code-specified loading protocol [12]. Test parameters were IFS sizes and material properties of the beam, made by either the ASTM A572 Gr. 50 or A36 steel. The ER70S-G electrode, which is similar to the high-toughness E71T-8 or E70TG-K2 electrodes, was used to make beam flange groove welds in all specimens. Ultrasonic tests (UT) were conducted for all flange groove welds, and they all satisfied the prescribed acceptance criteria [17]. Steel backing was left in place for the top and bottom flanges and no fillet welds were made between the steel backing and column face. Web joints were made with only slip-critical, high-strength bolts connecting the beam web to a shear tab welded to the column face. Finite element models of specimens were prepared using solid elements to verify IFS effectiveness and identify the possible sources of failure mode. The following conclusions are based on experimental results and associated analytical studies.

1. Specimen UR used a welded-unreinforced flange-bolted web connection. Although Specimen UR utilized the ASTM A36 beam and high-toughness flange groove welds, brittle fracture of the beam flange occurred before finishing the second cycle of 4% drift under the first cyclic test. It is expected that if the welded-unreinforced flange-bolted web connection had the ASTM A572 Gr. 50 beam, the connection failure would have occurred at a low drift.
2. Three IFS connection specimens, which had beam capacity–demand ratios larger than 1.05, experienced excellent performance and minor beam local buckling (e.g., low damage) under the first cyclic loading test up to a drift of 4%. These specimens were retested using the same loading protocol [12] and also experienced low damage in the beam up to a drift of 4%, leading to similar hysteretic responses as observed in the first cyclic test. Minor strength degradation due to beam buckling was noticed in the second test beyond drift of 4%. As long as the beam capacity–demand ratio, α (Table 2), was near 1.2 (e.g., Specimens IFS1 and IFS3), the IFS moment connection performed well in the second cyclic test up to a drift of 5–6%, irrespective of the ASTM A36 or A572 Gr. 50 steel beam.
3. Maximum moment developed at a quarter beam depth from the IFS end (plastic hinge location) was 1.25 and 1.48 times the actual plastic moment of the ASTM A572 Gr. 50 and A36 beams, respectively. The factor of around 1.5 for the ASTM A36 beam accounted for strain hardening that was accompanied by large inelastic

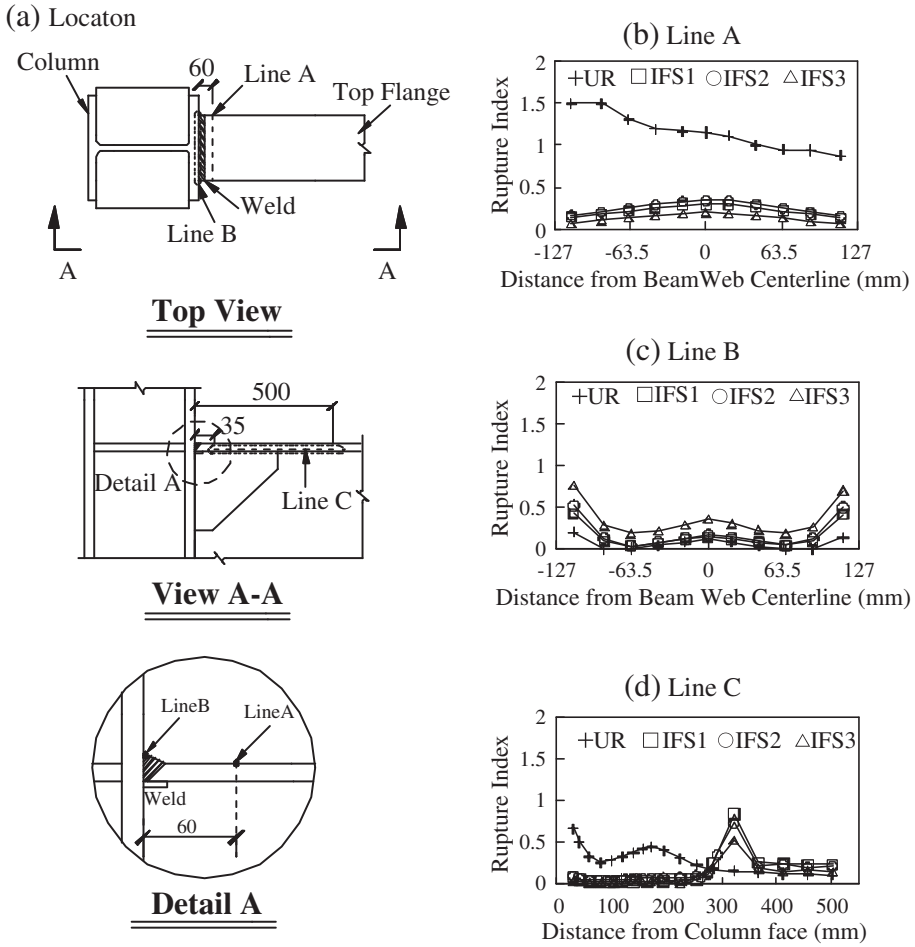

Fig. 15. Comparison of rupture index (RI) at a −4% drift.

deformations with minor beam buckling, and this value was higher than that calculated based on FEMA 350 [11].

4. Finite element analyses showed that the IFSs transferred about 20–25% connection moment to the column, lower than that obtained from the IFS moment connection with the built-up box column and wide-flange beam. The IFSs were effective in reducing the RI demands on the beam flange and groove-welded joint of the beam flange excluding both ends.

References

[1] Lu L-W, Ricles J, Mao C, Fisher J. Critical issues in achieving ductile behavior of welded moment connections. J Constr Steel Res 2000;55:325–41.
[2] Nakashima M, Roeder CW, Maruoka Y. Steel moment frames for earthquakes in Unites States and Japan. J Struct Eng ASCE 2000;126(8):861–8.
[3] Chi B-C, Uang C-M, Chen A. Seismic rehabilitation of pre-northridge steel moment connections: a case study. J Constr Steel Res 2006;62:783–92.
[4] Kim T, Stojadinovic B, Whittaker A. Seismic performance of pre-Northridge welded steel moment connections to built-up box columns. J Struct Eng ASCE 2008;134(2):289–99.
[5] Engelhardt MD, Winneberger T, Zekany AJ, Potyraj T. The dogbone connection: part II. Mod steel constrAISC; 1996.
[6] Uang C-M, Yu Q-S, Noel S, Gross J. Cyclic testing of steel moment connections rehabilitated with RBS or welded haunch. J Struct Eng ASCE 2000;126(1):57–68.
[7] Yu Q-S, Uang C-M, Gross J. Seismic rehabilitation of steel moment connections with welded haunch. J Struct Eng ASCE 2000;126(1):69–78.
[8] Chou C-C, Uang C-M. Cyclic performance of a type of steel beam to steel-encased reinforced concrete column moment connections. J Constr Steel Res 2002;58:637–63.
[9] Kim T, Whittaker AS, Gilani ASJ, Bertero VV, Takhirov SM. Cover-plate and flange-plate steel moment-resisting connections. J Struct Eng ASCE 2002;128(4):474–82.
[10] Lee CH. Seismic design of rib-reinforced steel moment connections based on equivalent strut model. J Struct Eng ASCE 2002;128(No. 9):1121–9.
[11] Federal Emergency Management Agency (FEMA). Recommended seismic design criteria for new steel moment-frame buildings. Rep. No. FEMA 350. Washington, D.C.: Federal Emergency Management Agency; 2000
[12] American Institute of Steel Construction (AISC). Seismic provisions for structural steel buildings, Chicago, IL; 2010.
[13] Chou C-C, Jao C-K. Seismic rehabilitation of welded steel beam-to-box column connections utilizing internal flange stiffeners. Earthquake Spectra 2010;26(4):927–50.
[14] Chou C-C, Tsai K-C, Wang Y-Y, Jao C-K. Seismic rehabilitation performance of steel side plate moment connections. Earthquake Eng Struct Dyn 2010;39:23–44.
[15] HKS. ABAQUS user's manual version 6.3. Pawtucket, RI: Hibbitt, Karlsson & Sorensen; 2009.
[16] ASTM. Specification for structural steel. Philadelphia, PA: American Society for Testing and Materials; 1988.
[17] Structural welding code-steel. Miami, Fla: Am. Welding Soc; 2006.
[18] Chou C-C, Wu C-C. Performance evaluation of steel reduced flange plate moment connections. Earthquake Eng Struct Dyn 2007;36:2083–97.
[19] Hancock JW, Mackenzie AC. On the mechanism of ductile fracture in high-strength steel subjected to multi-axial stress states. J Mech Phys Solids 1976;24:147–69.